

Subatomic-scale force vector mapping above a Ge(001) dimer using bimodal atomic force microscopy

Yoshitaka Naitoh^{1*}, Robert Turanský², Ján Brndiar², Yan Jun Li¹, Ivan Štich^{2,3,4*}
and Yasuhiro Sugawara¹

Probing physical quantities on the nanoscale that have directionality, such as magnetic moments, electric dipoles, or the force response of a surface, is essential for characterizing functionalized materials for nanotechnological device applications^{1–3}. Currently, such physical quantities are usually experimentally obtained as scalars. To investigate the physical properties of a surface on the nanoscale in depth, these properties must be measured as vectors. Here we demonstrate a three-force-component detection method, based on multi-frequency atomic force microscopy on the subatomic scale^{4–9} and apply it to a Ge(001)-c(4 × 2) surface. We probed the surface-normal and surface-parallel force components above the surface and their direction-dependent anisotropy and expressed them as a three-dimensional force vector distribution. Access to the atomic-scale force distribution on the surface will enable better understanding of nanoscale surface morphologies, chemical composition and reactions^{10,11}, probing nanostructures via atomic or molecular manipulation^{12,13}, and provide insights into the behaviour of nano-machines on substrates^{14,15}.

Noncontact atomic force microscopy (AFM) is an excellent tool not only for characterizing the atomic order on a surface but also for detecting the exchange, electrostatic, and chemical force interactions between the AFM tip and the sample surface^{16–19}. However, the conventional AFM, in which the force sensor oscillates perpendicular to the surface, reflects only the surface-normal component of the tip force and ignores the surface-parallel components. Although the parallel component of force has been calculated from the normal component using a potential mapping extraction technique, this method is only indirect^{20–24}. To obtain the distribution of the parallel components in three-dimensions (3D) with a higher accuracy, the force sensor should be oscillated also in the direction parallel to the surface^{25,26}. Recently, a multi-frequency AFM method was developed⁴ with the quest to investigate the physical properties of materials in deeper detail^{5,6}. This method utilizes both flexural and torsional modes of the cantilever, thereby making it useful for determining the force in a vector form by allowing the surface-normal (Z direction) and one of the surface-parallel force components (along the X or Y direction) to be simultaneously measured⁹.

Here we propose to detect all three components (X , Y and Z) of the total tip–surface force. For that purpose we use a clean Ge(001) surface. The surface has alternately aligned buckling dimers that form an anisotropic $c(4 \times 2)$ structure even at room temperature¹⁹.

As shown in Fig. 1, this surface has a structure wherein two domains are separated by a single step; across this step, the dimers are at an angle of 90° to each other. Therefore, both X and Y surface-parallel components of the tip–surface interaction can be obtained from both domains without the need to rotate the tip or the sample²⁶. Thus, the normal (Z) and both parallel (X and Y) components of the force interaction above the Ge(001)- $c(4 \times 2)$ surface can be obtained with this bimodal AFM method by measuring the flexural frequency shift Δf_{F} simultaneously with the two torsional frequency shifts Δf_{Tx} and Δf_{Ty} . Hereafter, the X and Y directions correspond to the dimer and dimer row directions, respectively.

We now demonstrate the consistency of our approach and compare experimental results with simulations. First, to determine how the normal (F_z) and the parallel (F_x and F_y) components of the tip–surface force are distributed above the surface, we compare the Z -dependence of the force component maps. Figure 2a,c shows F_z and F_x maps on the XZ plane ($1.6 \times 0.4 \text{ nm}^2$) based on data collected above dimer atoms along the X direction depicted by a ball model in the lower section of Fig. 2e. Figure 2b,d, shows F_z and F_y maps on the YZ plane ($1.2 \times 0.4 \text{ nm}^2$) based on data collected above atoms in a dimer row along the Y direction. In all maps, red and blue indicate the relative strength of the force fields in the vicinity of the surface, which decay steeply with increasing Z distance. There is a strong tip–surface force field between $Z = 0$ and 120 pm. In this strong force field regime, F_x and F_y are ~ 100 and 50 pN, respectively, around the dimer atom, which is smaller than F_z (~ 300 pN). This is in agreement with the findings in the previous study, which calculated the parallel and normal force fields on the XZ plane above a highly oriented pyrolytic graphite surface using bimodal AFM data⁹.

Furthermore, the obtained maps do not merely show the force magnitude distribution—they also include information on the force direction. In the strong force field regime of the F_z maps, small and large blue peaks indicate the downward force above the buckling down dimer atom (Bd) and buckling up dimer atom (Bu), respectively. We note that these images are consistent with results of a conventional AFM study¹⁹. In the F_x and F_y maps, however, the values approach zero (white colour) for the surface atoms. In addition, both F_x and F_y feature asymmetrically positive and negative extremal values (red and blue peaks) around the surface atoms, meaning the parallel force components reverse the direction on both sides of the surface atoms²⁶. Interestingly, at the centre of a dimer in the F_x mappings, the force field is weak (~ 50 pN) and

¹Department of Applied Physics, Osaka University, Yamada-oka 2-1, Suita 565-0871, Japan. ²CCMS, Institute of Physics, Slovak Academy of Sciences, 84511 Bratislava, Slovakia. ³Institute of Informatics, Slovak Academy of Sciences, 845 07 Bratislava, Slovakia. ⁴Department of Natural Sciences, University of Ss. Cyril and Methodius, 917 01 Trnava, Slovakia. *e-mail: naitoh@ap.eng.osaka-u.ac.jp; ivan.stich@savba.sk

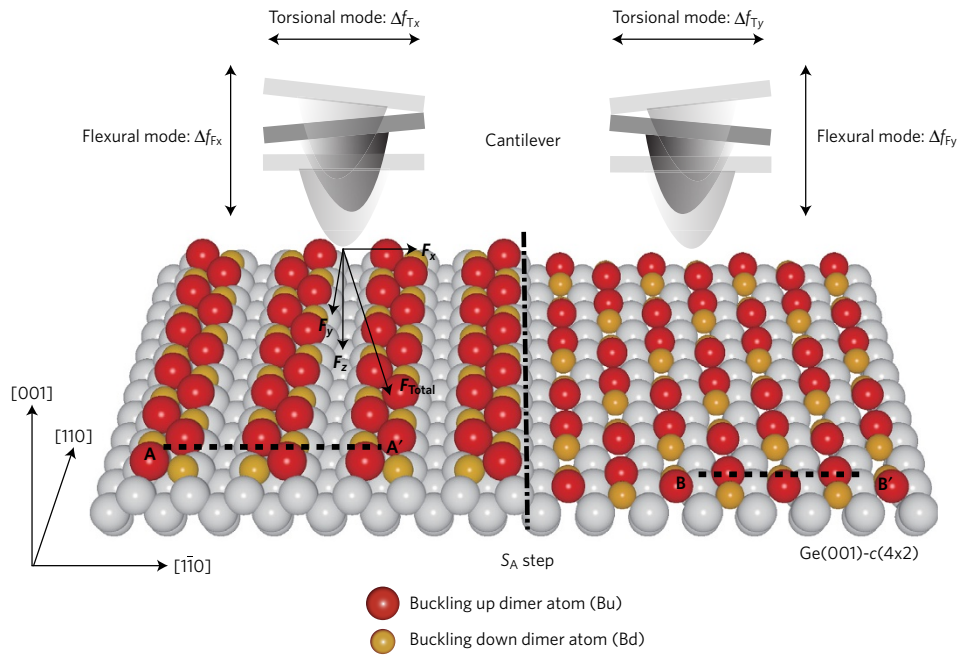


Figure 1 | Schematic of the 3D force detection method on a Ge(001)-c(4 × 2) surface using bimodal AFM. The cantilever oscillates at both flexural and torsional resonance frequencies to probe the normal (Z) and one of the parallel (X or Y) components of the interaction, respectively. The surface is schematically illustrated by a ball model with one S_A step, where red, orange and silver balls depict buckling up/buckling down dimer atoms (Bu/Bd), and the atoms underneath, respectively. The buckling dimer structure of the surface is rotated by 90° across the step. The dimer row direction, which is assigned to the Y direction, on the right terrace is parallel to the $[1\bar{1}0]$ direction and parallel to the $[110]$ direction on the left terrace. With this surface structure all X, Y and Z components of the tip-surface interaction forces, F_x , F_y and F_z , can be conveniently determined from the measured Δf_{Tx} , Δf_{Ty} and Δf_{Fx} (or Δf_{Fy}) data.

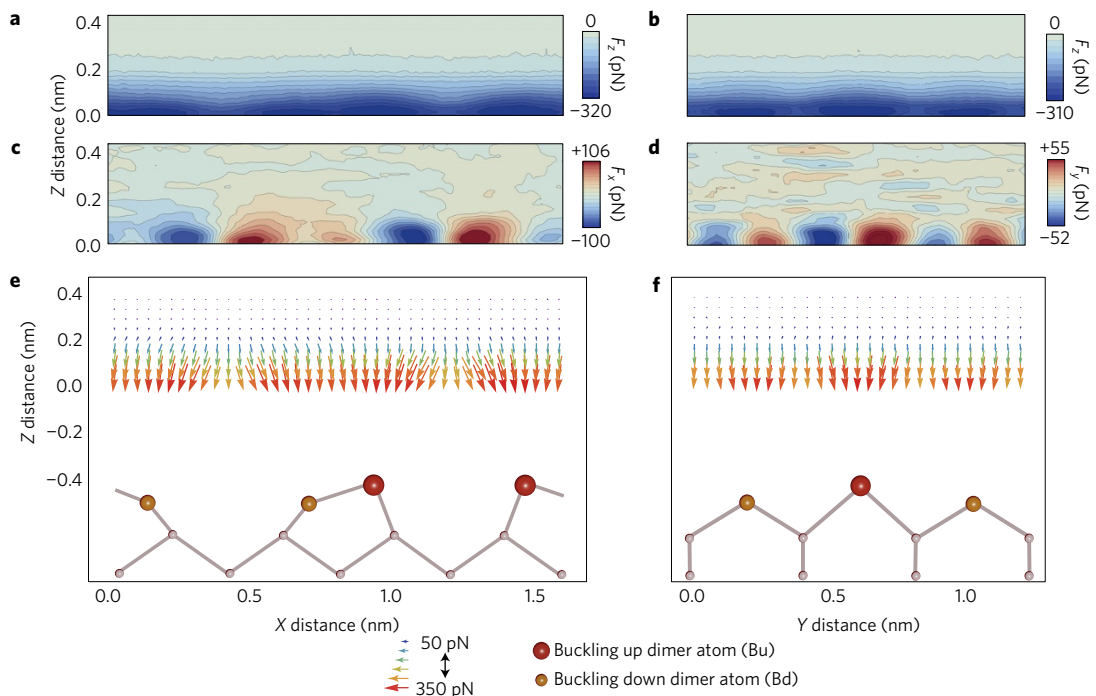


Figure 2 | Force component maps and force vector distributions above Ge(001) dimers. **a, c.** Maps of the Z and X components of the tip-surface total force, F_z and F_x , on the XZ plane ($1.6 \times 0.4 \text{ nm}^2$), collected above the A-A' line (see Fig. 1). **b, d.** Maps of the Z and Y components of the tip-surface total force, F_z and F_y , on the YZ plane ($1.2 \times 0.4 \text{ nm}^2$), collected above the B-B' line (see Fig. 1). **e, f.** Two-dimensional force vector (F_x , F_z) maps on the XZ plane and (F_y , F_z) maps on the YZ plane above the A-A' and B-B' lines, respectively. The ball and bar models of the dimer structure are shown in the lower section of the image with the atomic positions estimated from the force vector directions.

points toward the Bu, the reason being that the force field from the Bu overcomes that from the Bd due to the dimer structural height difference of 76 pm (ref. 27) between the Bu and Bd.

Figure 2e,f, shows a two-dimensional force vector field with the (F_x , F_z) and (F_y , F_z) distributions on the XZ and YZ planes, respectively. The force vectors are seen to point toward the surface

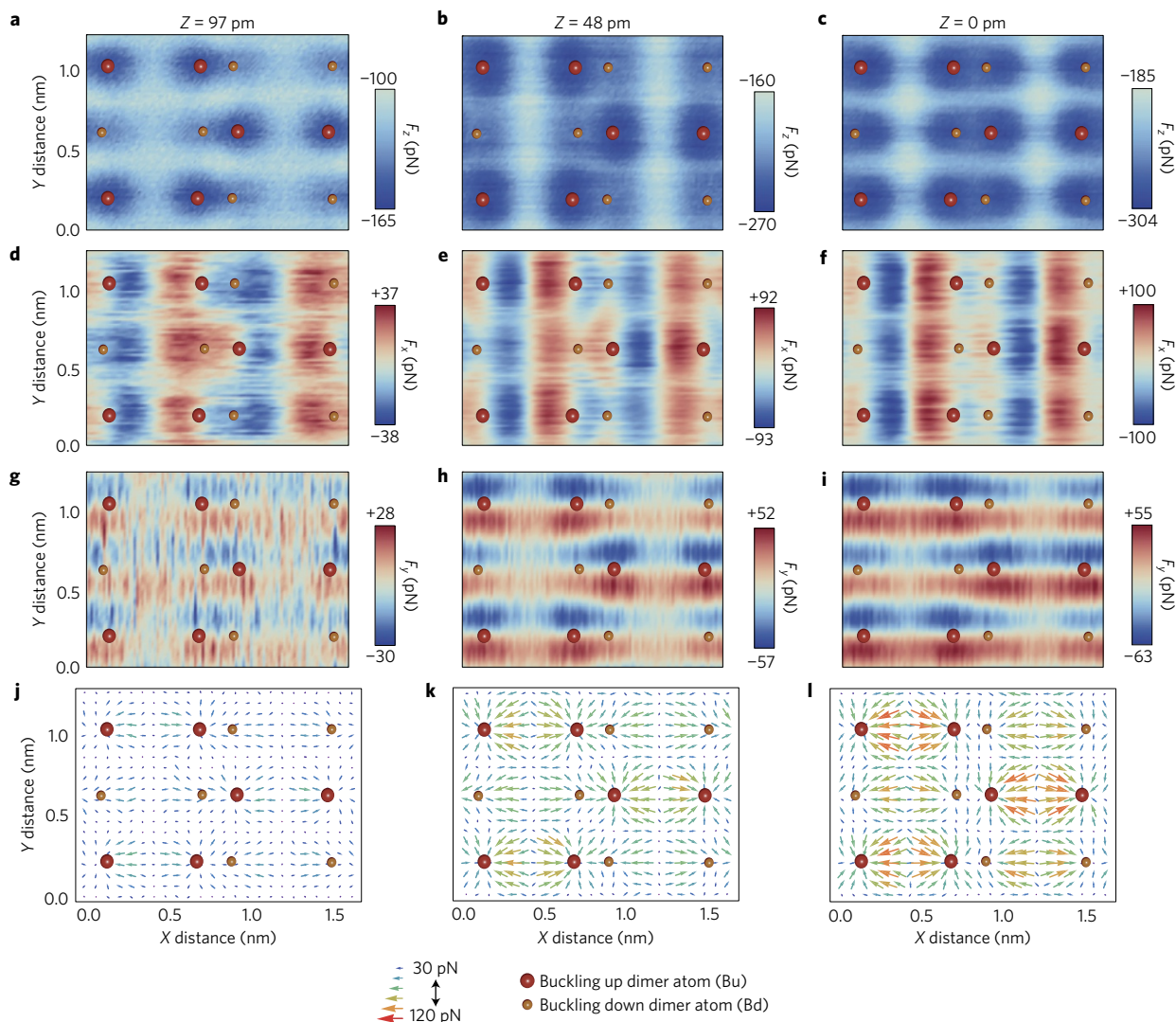


Figure 3 | Force component mappings and lateral force vector distributions on the Ge(001)-c(4 × 2) surface. **a–c**, Maps of the normal (Z) component of the total force, F_z , on the XY plane of an area comprising six dimers ($1.6 \times 1.2 \text{ nm}^2$). **d–i**, Parallel (X and Y) components of the total force maps on the same XY plane (F_x map (**d–f**) and F_y map (**g–i**)). The force map series **a–c**, **d–f**, and **g–i**, were obtained at $Z = 97$, 48, and 0 pm, respectively. The red and blue areas indicate that the force component direction is positive or negative, respectively. **j–l**, Two-dimensional lateral force vector (F_x , F_y) distributions at the same height on the same area of the XY plane reproduced from the lateral force data, F_x and F_y . For reference, the Bu and Bd positions are shown by superimposed red and orange balls.

atoms, as intuitively expected in the strong attractive force field. This also means that our unique ability to experimentally determine the 3D force field can be used to estimate the surface atom position, its height below the tip in particular, directly from the measured force vector directions (see the Supplementary Information for details). In Fig. 2e,f, the dimer atom structure models are shown with the Bu location so determined at ~ 420 pm below the $Z = 0$ position. In both maps in the strong force field regime the force vector magnitude is ~ 330 pN at the Bu site and ~ 300 pN at the Bd site. The areas with the strongest force vectors are symmetrically distributed on each dimer atom (Fig. 2f). However, the area with the strongest forces in Fig. 2e deviates by $18^\circ \pm 2^\circ$ to the outside of the dimer from the surface-normal direction on the Bu site and by $15^\circ \pm 2^\circ$ on the Bd site. The deviations are caused by the weak parallel force field above the dimer and by the directionality of the dangling bonds on the Bu and Bd (see also the Supplementary Information for computed charge densities on the dimers). In summary, we have demonstrated that the tip–surface force vector distribution and its directionality, which reflects the surface anisotropy, can be detected on the subatomic scale.

Next, to study the distribution of each component in the strong force field area of the surface we determine the complete F_x , F_y , and F_z maps. Figure 3a–c shows the F_z maps on the XY plane for an area comprising six dimers ($160 \times 120 \text{ pm}^2$) at tip–surface Z distances of 97, 48 and 0 pm. At $Z = 97$ pm, strong and faint local minima (more and less negative values) are visible on the Bu and Bd sites, respectively (Fig. 3a). Both local minima deepen as the Z distance decreases (Fig. 3b), and F_z on the Bu site reaches the minimum value (~ 320 pN) near $Z = 15$ pm. At $Z = 0$ pm (Fig. 3c), the Bu and Bd sites have a similar image contrast.

In Fig. 3, panels d–f and g–i, respectively, display a series of F_x and F_y maps on the XY planes at Z distances identical to those in Fig. 3a–c. The F_x and F_y maps exhibit a stripe-like modulation with red and blue contrast (positive and negative values) along the X and Y directions, respectively. The modulation amplitudes increase as the Z distance is reduced. As can be observed in the force component maps in Fig. 3, the F_x and F_y values approach zero on the surface atoms, which are in good agreement with the result of previous studies^{15,26}. F_x and F_y have asymmetrically positive and negative extremal values around the surface atoms, which are

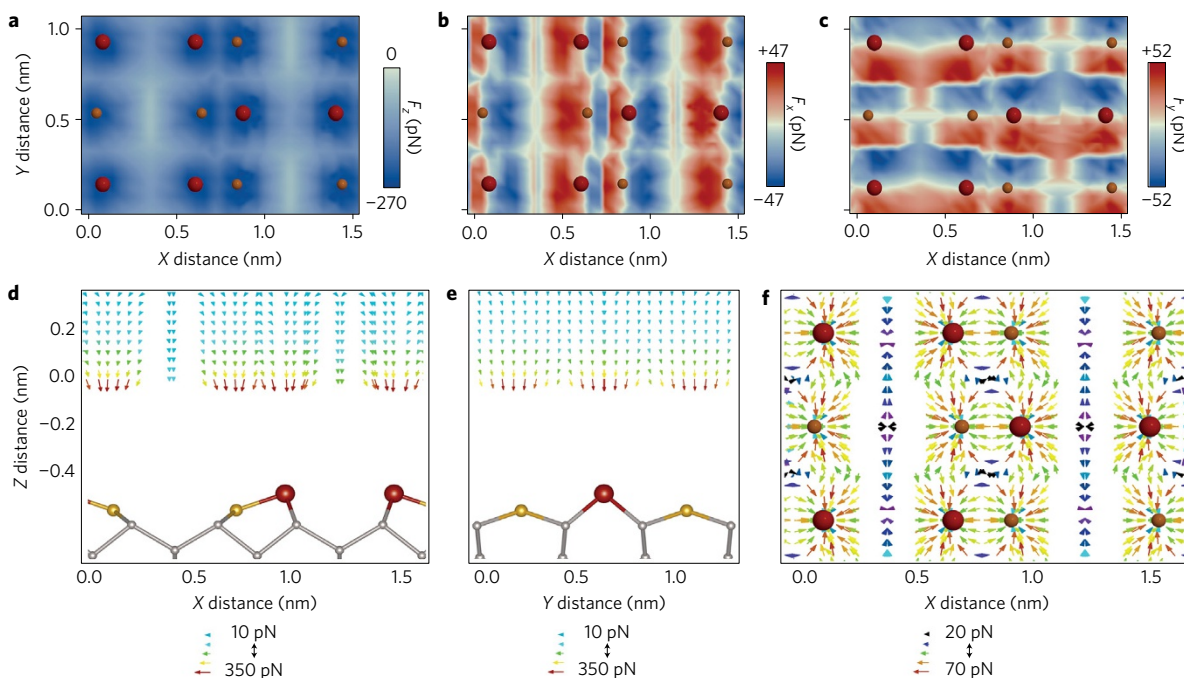


Figure 4 | Simulated force component mapping on the Ge(001)-c(4 × 2) surface. **a–c**, Simulated force mappings corresponding to the experimental images in Fig. 3c,f,i, respectively, calculated at $Z = 480$ pm, defined as the distance between the tip apex and the Bu site prior to relaxation. **d,e**, Two-dimensional force vector (F_x, F_z) maps on the XZ plane and (F_y, F_z) maps on the YZ plane above the A–A' and B–B' lines in Fig. 1, respectively, corresponding to the experimental images in Fig. 2e,f. **f**, (F_x, F_y) maps at the height of $Z = 480$ pm on the same area of the XY plane as in **a–c**, corresponding to the experimental results in Fig. 3l. Ball and bar models of the dimer structure are superimposed for clarity.

indicative of the force component direction reversal on both sides of the surface atom. Areas in which the force is zero are also observed around the median lines between neighbouring surface atoms. Their appearance indicates that the force fields from both sides cancel each other out at these locations. Therefore, the above results show that the parallel force components have a direction-dependent anisotropy on the surface (XY plane).

Figure 3j–i displays the two-dimensional lateral force vector (F_x, F_y) distributions on the XY planes at the same distances as the above maps. The force vector distributions reflect the directionality of the lateral force on the surface as well as the magnitude of the force. Most of the lateral force vectors are directed to the nearest surface atoms at any Z distance. This result is reasonable, as the value of the tip–surface force falls in the attractive range. Only above the centre area of a dimer does the vector around Bd site tend to point toward the partnered Bu site because the lateral force from Bd site is counteracted by the force from the partnered Bu site due to the asymmetric properties of the dimer. Therefore, the lateral force vector magnitude is greater outside a dimer, particularly near the Bu site, whose maximum value increases as the Z distance is reduced from 48 pN at $Z = 97$ pm to 118 pN at $Z = 0$ pm. In summary, we have successfully demonstrated the magnitude and direction of the tip–surface lateral force on a subatomic scale in a 3D space and visualized it as a vector distribution.

To understand the nature of the measured force vector mappings we have performed DFT simulations of 3D tip–surface interactions by directly calculating the force vectors acting on the tip²⁸. The most salient features of the experimental images are the dimers which are imaged as buckled at large tip–surface distances and as quasi-symmetric at shorter distances and the extremely small measured forces of ~ 30 –300 pN. For comparison, a typical tip–surface force corresponding to a covalent interaction on a reactive semiconductor surface is ~ 1 nN. Therefore, assuming a sharp W-terminated tip, the tip–surface distance must be significantly larger than a typical covalent bond distance of ~ 200 pm. This excludes a direct mechanism

of dimer symmetrization induced via the tip interaction with the Bd site which would lead to its lifting up as a result. Indeed, assuming this scenario leads to tip–surface distances of ~ 300 pm and tip–surface forces an order of magnitude larger than those measured experimentally (see the Supplementary Information for the simulated images in this regime). Hence, the tip–surface distance must be significantly larger. However, these assumptions lead to dimers appearing as asymmetric at all tip–surface distances (see the Supplementary Information). To reconcile the weak tip–surface forces with symmetric dimer appearance in the interaction regime around $Z \sim 0$ pm (Fig. 3c), we propose an indirect dimer symmetrization mechanism via tip-induced modification of the electronic structure, which in turn excites, via electron–phonon coupling, dimer rocking vibrations, which then induce their symmetric image appearance (see Supplementary Information for more details). Indeed, such a scenario in which the electronic π and σ dimer states couple with the dimer rocking vibrations was used to create dimer kinks on the Ge(001)-c(4 × 2) surface in STM experiments²⁹.

Taking the symmetrization effect into account and taking the W-terminated tip–surface distance to ~ 480 pm leads to the AFM force images shown in Fig. 4a–c, which compare very favourably with the experimental results for $Z = 0$ pm in Fig. 3c,f,i. The only quantitative difference from the experiment is the calculated F_x value smaller than experimentally measured, which we were able to trace back to the preselected model tip rotation with respect to the surface. Indeed, the tip–surface distance of ~ 480 pm, which gives the best agreement with the experimental results, is in line with the experimental estimates $\sim 420 \pm 60$ pm. Simulation of the weak and intermediate interaction regime (Fig. 3) force images at $Z = 98$ and 48 pm, was not attempted, as in the former the maximum experimental lateral forces are comparable to the achievable DFT accuracy of ~ 16 pN and in the latter quantification of the dimer symmetrization effect is not straightforward. Nonetheless, the proposed indirect distance-dependent tip–surface dimer symmetrization scenario applies equally also here. We have also

extracted the simulated 2D force vector maps on three characteristic planes, XZ, YZ and XY, shown in Fig. 4d–f, respectively, which again show an excellent agreement with experiments.

The described method of simultaneous measurement of the force vector distribution in a 3D space is available only for the special cases in which the sample surface has two domains rotated by 90°. For more general cases, including functional material surfaces with sub-nanoscale structures, the tip or the sample has to be rotated to detect both parallel force components on the surface. Hence, we suggest use of a tip or sample rotational device where the sample displacement is suppressed within a few micrometres after the rotation³⁰. Then the nanoscale positional recognition system³¹ will allow also in this more general case detection of the force vector distribution with subatomic resolution. It should be remembered that careful control of the tip or sample movement are required to avoid any modification of the tip apex structure. In addition, the tip apex element, which can be modified via the metal coating³², should be appropriately chosen considering its reactivity with the surface. For instance, platinum or iridium is more appropriate for metal oxide surfaces than tungsten. With these modifications, the bimodal AFM method can be applied to any functionalized surface.

Using a combination of experiments and DFT simulations we have demonstrated that the bimodal AFM method makes detection and understanding of the 3D tip–surface force field above the Ge(001)-c(4 × 2) surface and its expression on subatomic scale in the form of a vector distribution possible. With the proposed modification of the experimental set-up, the novel bimodal AFM technique has the potential to detect both the magnitude and direction of the tip–surface force and hence is expected to provide valuable information not only on chemical reactions and nanostructure formation on the substrate but also to provide new subatomic-scale insights on the friction and lubrication phenomena. Finally, keeping in mind the ability of bimodal AFM to access also the electronic and magnetic properties, the technique has the potential of opening up a new window also on investigation of functionalized surfaces.

Methods

Methods, including statements of data availability and any associated accession codes and references, are available in the [online version of this paper](#).

Received 22 June 2016; accepted 7 March 2017;
published online 10 April 2017

References

- Wolfe, S. A., Jiwei, L., Stan, M. R., Chen, E. & Treger, D. M. The promise of nanomagnetism and spintronics for future logic and universal memory. *Proc. IEEE* **98**, 2155–2168 (2010).
- Burghard, M., Klauk, H. & Kern, K. Carbon-based field-effect transistors for nanoelectronics. *Adv. Mater.* **21**, 2586–2600 (2009).
- Schmidt, R. *et al.* Probing the magnetic exchange forces of iron on the atomic scale. *Nano Lett.* **9**, 200–204 (2009).
- Rodriguez, T. R. & Garcia, R. Compositional mapping of surfaces in atomic force microscopy by excitation of the second normal mode of the microcantilever. *Appl. Phys. Lett.* **84**, 449–451 (2004).
- Garcia, R. & Herruzo, E. T. The emergence of multifrequency force microscopy. *Nat. Nanotech.* **7**, 217–226 (2012).
- Solaes, S. D. & Chawla, G. Triple-frequency intermittent contact atomic force microscopy characterization: simultaneous topographical, phase, and frequency shift contrast in ambient air. *J. Appl. Phys.* **108**, 054901 (2010).
- Naitoh, Y., Ma, Z. M., Li, Y. J., Kageshima, M. & Sugawara, Y. Simultaneously observation of surface topography and elasticity at atomic scale by multifrequency frequency modulation atomic force microscopy. *J. Vac. Sci. Technol. B* **28**, 1210–1214 (2010).
- Kawai, S. *et al.* Systematic achievement of improved atomic-scale contrast via bimodal dynamic force microscopy. *Phys. Rev. Lett.* **103**, 220801 (2009).
- Kawai, S. *et al.* Ultrasensitive detection of lateral atomic-scale interactions on graphite (0001) via bimodal dynamic force measurements. *Phys. Rev. B* **81**, 085420 (2010).
- Hickenboth, C. R. *et al.* Biasing reaction pathways with mechanical force. *Nature* **446**, 423–427 (2007).

- Felts, J. R. *et al.* Direct mechanochemical cleavage of functional groups from graphene. *Nat. Commun.* **6**, 6467 (2015).
- Custance, O., Perez, R. & Morita, S. Atomic force microscopy as a tool for atom manipulation. *Nat. Nanotech.* **9**, 803–810 (2009).
- Lee, G. *et al.* Nanomechanical characterization of chemical interaction between gold nanoparticles and chemical functional groups. *Nanoscale Res. Lett.* **7**, 608–618 (2012).
- Mo, Y., Turner, K. T. & Szlufarska, I. Friction laws at the nanoscale. *Nature* **457**, 1116–1119 (2009).
- Kawai, S. *et al.* Superlubricity of graphene nanoribbons on gold surfaces. *Science* **351**, 957–961 (2016).
- Morita, S., Wiesendanger, R. & Meyer, E. *Noncontact Atomic Force Microscopy* (Springer, 2002).
- Arima, E. *et al.* Magnetic force microscopy using tip magnetization modulated by ferromagnetic resonance. *Nanotechnology* **26**, 125701 (2015).
- Kou, L. *et al.* Surface potential imaging with atomic resolution by frequency-modulation Kelvin probe force microscopy without bias voltage feedback. *Nanotechnology* **26**, 195701 (2015).
- Naitoh, Y., Kamijo, T., Li, Y. J. & Sugawara, Y. Quantification of atomic-scale elasticity on Ge(001)-c(4 × 2) surfaces via noncontact atomic force microscopy with a tungsten coated tip. *Phys. Rev. Lett.* **109**, 215501 (2012).
- Ternes, M., Lutz, C. P., Hirjibehed, C. F., Giessibl, F. J. & Heinrich, A. J. The force needed to move an atom on a surface. *Science* **319**, 1066–1069 (2008).
- Sugimoto, Y., Namikawa, T., Miki, K., Abe, M. & Morita, S. Vertical and lateral force mapping on the Si(111)-(7 × 7) surface by dynamic force microscopy. *Phys. Rev. B* **77**, 195424 (2008).
- Ruschmeier, K., Schirmeisen, A. & Hoffmann, R. Atomic-scale force-vector fields. *Phys. Rev. Lett.* **101**, 156102 (2008).
- Albers, B. J. *et al.* Three-dimensional imaging of short-range chemical forces with picometre resolution. *Nat. Nanotech.* **4**, 307–310 (2009).
- Weymouth, A. J., Hofmann, T. & Giessibl, F. J. Quantifying molecular stiffness and interaction with lateral force microscopy. *Science* **343**, 1120–1122 (2014).
- Kawai, S., Sasaki, N. & Kawakatsu, H. Direct mapping of the lateral force gradient on Si(111)-7 × 7. *Phys. Rev. B* **79**, 195412 (2009).
- Weymouth, A. J. *et al.* Atomic structure affects the directional dependence of friction. *Phys. Rev. Lett.* **111**, 126103 (2013).
- Tütüncü, H. M., Jenkins, S. J. & Srivastava, G. P. Atomic geometry, electronic structure, and vibrational properties of the Ge(001)(2 × 1) surfaces. *Phys. Rev. B* **57**, 4649–4655 (1998).
- See, for instance Bamidele, J. *et al.* Chemical tip fingerprinting in scanning probe microscopy of an oxidized Cu(110) surface. *Phys. Rev. B* **86**, 155422 (2012).
- Tomatsu, K. *et al.* Local vibrational excitation through extended electronic states at a germanium surface. *Phys. Rev. Lett.* **103**, 266102 (2009).
- Yoshida, K., Nishi, R. & Mori, H. *Design of High-Speed Tomography with the 3MV Ultrahigh Voltage Electron Microscope* EMC 2008 14th European Microscopy Congress Vol. 1, 341 (2008).
- Higuchi, S. *et al.* Multiple-scanning-probe tunneling microscope with nanoscale positional recognition function. *Rev. Sci. Instrum.* **81**, 073706 (2010).
- Kinoshita, Y., Naitoh, Y., Li, Y. J. & Sugawara, Y. Fabrication of sharp tungsten-coated tip for atomic force microscopy by ion-beam sputter deposition. *Rev. Sci. Instrum.* **82**, 113707 (2011).

Acknowledgements

We are grateful to L. Kantorovich, King's College London, and T. Glatzel, University of Basel, for their valuable contributions. This work was supported by a Grant-in-Aid for Scientific Research (B) (Grant No. 26286007) from JSPS, Grant-in-Aid for Exploratory Research (Grant No. 15K13275) from JSPS, APVV-0759-15, VEGA 2/0162/15, and by V4-Japan Joint Research Program on Advanced Materials (NaMSeN) projects. We also gratefully acknowledge use of the Hitachi SR16000/M1 supercomputer system at CCMS/IMR, Tohoku University, Japan.

Author contributions

Y.N. and Y.S. conceived 3D force vector mapping using bimodal AFM. Y.N. performed the AFM experiments and analysed the data. R.T., J.B. and I.S. performed DFT calculations. Y.N. and I.S. wrote the paper. All authors discussed the results and commented on the manuscript.

Additional information

Supplementary information is available in the [online version of the paper](#). Reprints and permissions information is available online at www.nature.com/reprints. Publisher's note: Springer Nature remains neutral with regard to jurisdictional claims in published maps and institutional affiliations. Correspondence and requests for materials should be addressed to Y.N. or I.S.

Competing financial interests

The authors declare no competing financial interests.

Methods

All experiments were performed using our custom atomic force microscopy apparatus equipped with an optical fibre interferometer system operating at room temperature under ultrahigh vacuum (UHV) below 3×10^{-9} Pa (ref. 33). The cleaned Ge(001) surface (As-doped, 0.5–0.6 Ω cm) was obtained via several cycles of Ar⁺ sputtering at 1 keV followed by annealing at 973–1,073 K in the UHV chamber. As a force sensor, a commercial Si cantilever (Tap190Al-G, BudgetSensors) was adopted. Prior to the AFM experiments, the cantilever tip was cleaned by Ar⁺ sputtering to remove the oxidized layer and was then uniformly covered by tungsten via sputter-coating in the UHV chamber³². The cantilever was simultaneously oscillated at the second flexural resonant frequency ($f_f = 909$ kHz) and the fundamental torsional resonant frequency ($f_t = 1.29$ MHz). The oscillation amplitudes of the two modes, A_f and A_t , were maintained at 420 pm and 35 pm, respectively, using phase-locked-loop electronics (HFL12, Zurich Instrument). The tip–surface force interaction was detected using the frequency modulation technique—that is, the flexural and torsional frequency shifts, Δf_f and Δf_t , were detected simultaneously. Both frequency shifts were measured in the spatial area of $4.0 \times 4.0 \times 1.6$ nm³ above the surface. All three components of the total force, F_x , F_y and F_z , were calculated from the obtained frequency shift data, Δf_{Tx} , Δf_{Ty} and Δf_{Tz} , by first converting them to time-averaged force components with the Z component ascribed to the virtual component with zero lateral oscillation amplitude with accuracy better than 93%. F_z was determined by subtracting the long-range force contribution. F_x and F_y were acquired by integrating the time-averaged components along the vibratory direction. More details can be found in Supplementary Information.

In our calculations the surface was modelled using an eight-layer Ge-slab H-terminated at the bottom with the upper six atomic layers allowed to relax. We have used a supercell consisting of four $c(4 \times 2)$ elementary cells. Several tip

models have been tested (see Supplementary Information for more details), and a simple pyramidal (BCC (100)) tungsten model tip was used in the simulations. Calculations of the energies and forces were performed using density functional theory (DFT) with projector augmented-wave pseudopotentials³⁴ and a 250 eV plane wave cut-off as implemented in the VASP code³⁵. Most calculations were done using the Perdew–Burke–Ernzerhof (PBE)³⁶ exchange–correlation functional, with a smaller set of calculations performed with the hybrid Heyd–Scuseria–Ernzerhof (HSE06)³⁷ exchange–correlation functional. Convergence of ionic forces to accuracy better than 16 pN was used as a convergence criterion. More details can be found in Supplementary Information.

Data availability. The data that support the mappings within this paper and other findings of this study are available from the corresponding authors upon reasonable request.

References

- Suehira, N., Tomiyoshi, Y., Sugawara, Y. & Morita, S. Low-temperature noncontact atomic-force microscope with quick sample and cantilever exchange mechanism. *Rev. Sci. Instrum.* **72**, 2971–2976 (2001).
- Blöchl, P. E. Projector augmented-wave method. *Phys. Rev. B* **50**, 17953–17979 (1994).
- Kresse, G. & Furthmüller, J. Efficiency of ab-initio total energy calculations for metals and semiconductors using a plane-wave basis set. *J. Comput. Mater. Sci.* **6**, 15–50 (1996).
- Perdew, J. P., Burke, K. & Ernzerhof, M. Generalized gradient approximation made simple. *Phys. Rev. Lett.* **77**, 3865–3868 (1996).
- Heyd, J., Scuseria, G. E. & Matthias Ernzerhof, M. Hybrid functionals based on a screened Coulomb potential. *J. Chem. Phys.* **118**, 8207–8215 (2003).